CHAPTER 4

ANN APPROACH FOR SYSTEM IDENTIFICATION OF STRUCTURES

4.1 Introduction

System identification is an essential means of studying the dynamic characteristics of a structural system. In conventional ways, there have been a number of effective identification methods which can be found in lots of books [89, 90] or articles for a linear dynamic system. For a nonlinear dynamic system, in contrast, few effective methods are available. Some existing methods which require prior knowledge or rely on certain assumptions, may only work for specific types of nonlinearities. A main difficulty in dealing with a nonlinear system lies in finding a reliable mathematical model for it. Without a model, it is usually impossible to proceed with system identification. Neural network, however, does not rely on a preconceived mathematical model or even the number of parameters. Owing to its brilliant learning capability and its nonlinear nature, neural network is well suited for nonlinear system identification and was studied and applied to real-world problems [10, 12, 13, 52, 53, 56, 91].

The operation of neural networks in system identification for either a linear system or a nonlinear system is the same. The neural networks are trained from the

observed input-output data of the dynamic system to be identified. Thus, the trained network reflects the input-output characteristics of the system it intends to represent. If the input-output data is well formed and meaningful in physical way, a trained neural network has the capacity to stand for the structural system in dynamics.

In the following sections, a general view on the application of neural networks in system identification is first introduced. Subsequently, the theoretical basis and operation of the developed system identification model (named as ANNSI model) which is based on the combination of the time-domain analysis method and an artificial neural network is presented. The ANNSI model can be used to obtain the modal parameters of structures from the structural acceleration or strain measurements. The global and decentralized system monitoring networks, which are used for health monitoring purposes, are also presented in turn. In addition, examples are also performed right after the models or methods are presented to exam the capabilities of each of them.

4.2 General View On Application Of ANN In System Identification

To find a network topology (or structure) that suitable for modeling the real structural system is the essence of using neural networks for system identification. As a result, with the same inputs, a trained neural network should produce similar outputs as the real system does within an acceptable error range. When using neural network for system identification of a structural system, the following general characteristics should be addressed.

(1) There is no need to establish a mathematical model for the real dynamic

system, since the operation of a neural network is basically treated as a 'black box'. This is particularly attractive for the nonlinear system identification because it is usually difficult to establish a mathematical model for such a system. The learning process of a neural network is implemented basing on the input-output data from a real system. Therefore, only the input-output relationship of such a system is studied. The dynamic characteristics or system parameters are reflected by the connective weights in the neural network.

(2) Despite the advantages of using neural network in system identification, an inherent inconvenience is that the topology of the network (i.e. the numbers of layers and neurons, and the transfer function adopted) is usually searched by empirical and trial-and-error methods. The network topology is also selected based on the compromise between the identification accuracy and the complexity of the network. When simple network topology is employed (without or with only one hidden layer and linear transfer function is used, for example), lesser learning cost and lower identified accuracy is yielded. On the contrary, a complicated network topology (more than one hidden layer and nonlinear transfer function is involved, for example) leads to more burdensome learning time and higher accuracy. From this viewpoint, the selection of a suitable network topology for system identification seems a burden in some aspects. Fortunately, with more understanding about the behaviors of the system, the selection of the network topology would be easier and more appropriate.

(3) The convergence rate of the identification network is overwhelmingly

dictated by the network topology, the learning algorithm, and the training information employed, but rarely depended on the dimension of the system.

(4) Trained neural network as an identification model is a physical realization of a real system. It can be used for further related applications, such as on-line control, damage detection, and health monitoring of structural system.

Two ways of learning, with and without feedback inputs, are commonly adopted for system identification using neural network. Figures 4.1 and 4.2 diagrammatically illustrate the principle of these two learning approaches, respectively.

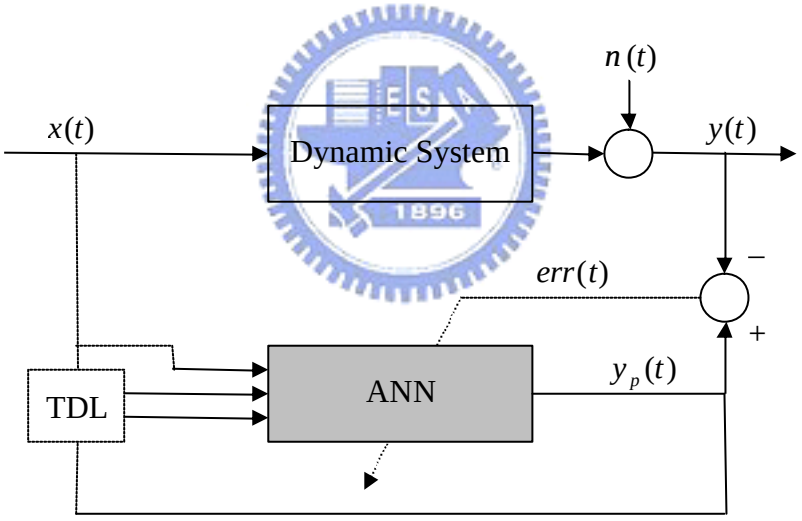

Figure 4.1 Identification network trained with feedback inputs

As shown in Figure 4.1, the terms, $x(t)$, $y(t)$, and $n(t)$, are the generalized input, output, and noise of the dynamic system at time *t*, respectively. The term, $y_p(t)$, is the predicted output from the network. The generalized input and output could be

any kind of structural responses, such as displacement, velocity, acceleration, and even strain. TDL stands for tapped delay line which provides a phase delay for a signal. In a training iteration, the connective weights of the network are adjusted based on the discrepancy, $err(t)$, between the predicted output ($y_p(t)$) from the neural network and real output ($y(t)$) of the system. In addition, the predicted output is feedback to the input layer as a part of the training input data for the next training iteration.

In the similar way, a neural network can be trained for system identification without feedback inputs (as shown in Figure 4.2). This way of learning is most adopted for its simplicity and fast convergence. Throughout this research, the neural networks are trained in this way.

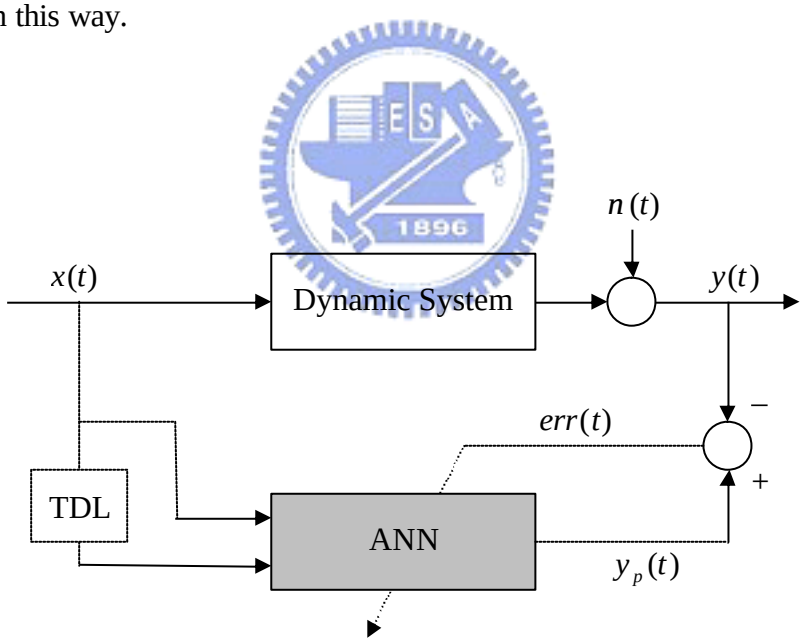

Figure 4.2 Identification network trained without feedback inputs

4.3 ANNSI Model For Modal Analysis

The development of experimental modal analysis as a new technology is propelled by its ability to offer quick and effective solutions to practical engineering problems. Along with the development of modern computer technology, experimental modal analysis has become the main tool for solving complicated structural vibration problems. For an existing engineering structure, experimental modal analysis provides vital information on its dynamic behavior, thus permitting intelligent solutions to vibration problems the structure may be experiencing.

This section presents a novel modal analysis approach, ANNSI model, for the identification of structural modal parameters (such as natural frequencies, modal damping ratio, and mode shapes) of structures. The dynamic characteristics are directly evaluated from the weighting matrices of the neural network trained by observed structural responses and input base excitations. This model is constructed based on a supervised neural network and a time series analysis method [13]. Theoretically, various kinds of structural responses can be used in this model. For the convenience of interpretation, however, the most measured response, acceleration, is employed to develop the formulation in the ANNSI model.

4.3.1 Construction of Modal Analysis Network (MAN) for a Linear Dynamic System

Acceleration responses are normally measured in monitoring the responses of a structure in an earthquake. Therefore, these measured data are used to train an ANN. Figure 4.3 illustrates the proposed structure of the ANN, where $f_l(t-i)$, with

$i = 0, 1, 2, \cdots n$, represents input base accelerations, corresponding to component l at $(t-i)$ time step, while $\ddot{x}_k(t-j)$, with $j = 0, 1, 2, \cdots m$, represents the observed acceleration responses of the kth degree of freedom (DOF) relative to the base at the $(t-j)$ time step. It is seen from Figure 4.3 that, the structural response at current moment is correlated with the structural response and system inputs at previous moments. As a result, this network model is similar to the time series ARX model.

Herein, a nonlinear transfer function is used in the network and is defined as,

$$g(y) = \begin{cases} 1 & when\ y > 1 \\ y & when\ -1 \le y \le 1 \\ -1 & when\ y < -1 \end{cases} \tag{4.1}$$

Notably, the values for nodes in the input layer are usually normalized to the range between 1 and –1 in training an ANN. Consequently, the argument of the transfer function is rarely larger than 1 or less than –1.

Following the procedure for establishing a neural network and using the observed acceleration responses of the target structure in an earthquake, enables the connective weights and thresholds to be determined and an appropriate network topology to be established for the structural system.

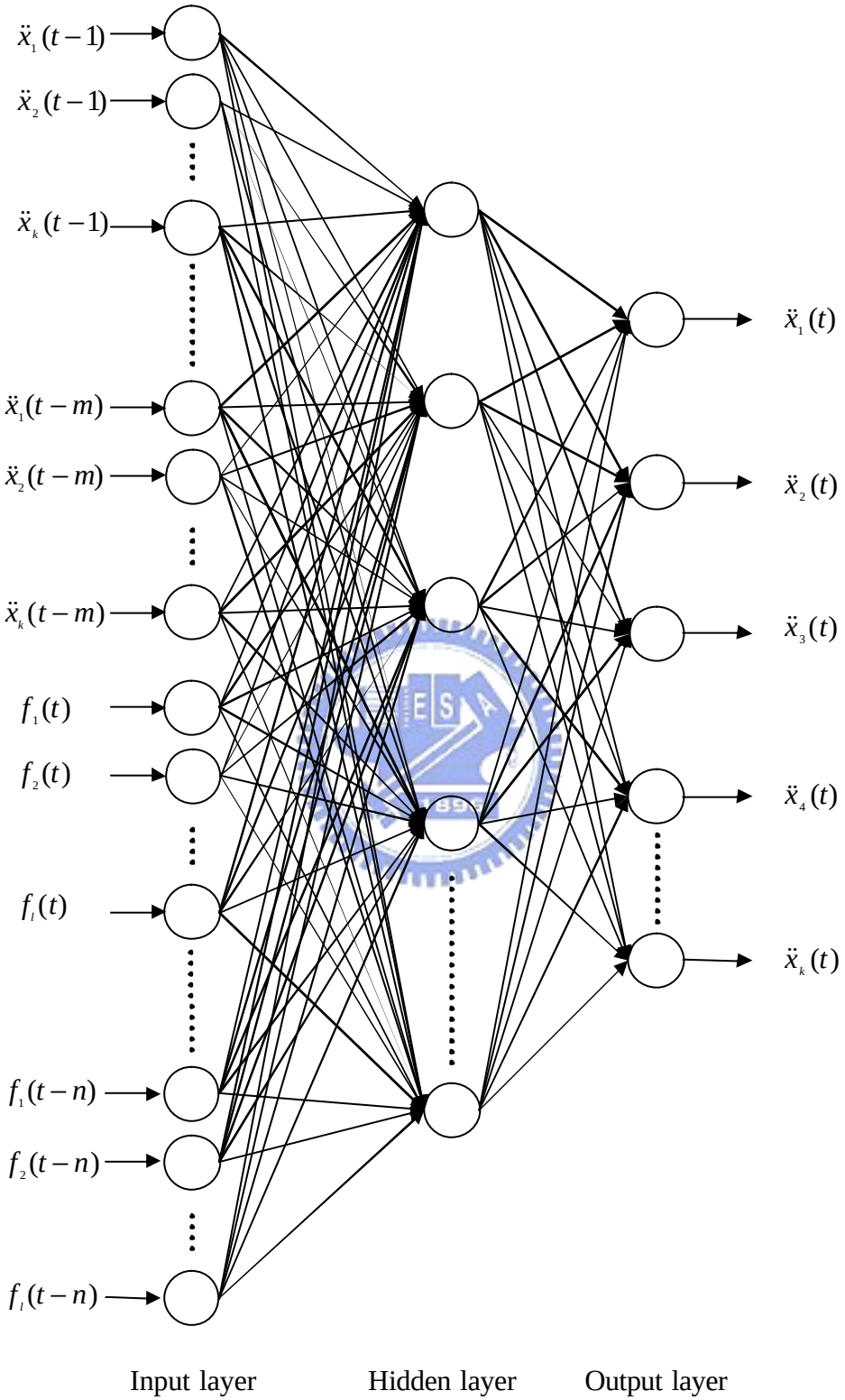

Figure 4.3 Topology of the modal analysis neural network

Careful investigation of the ANN established according to Figure 4.3 reveals that the network yields a linear system if the transfer function is linear. The normalization of the values in the input nodes is such that the responses in the output layer are approximately related to the values of the input nodes by the following linear relationship.

$$\{Y\} = [W][V]\{X\} + ([W]\{q_v\} + \{q_w\}) \tag{4.2.a}$$

where

$$\{Y\} = [\ddot{x}_1(t), \ddot{x}_2(t), \cdots, \ddot{x}_k(t)]^T \tag{4.2.b}$$

$$\{X\} = [\overline{\mathbf{X}}\ \mathbf{F}]^T \tag{4.2.c}$$

$$\begin{aligned}\overline{\mathbf{X}} = [&\ddot{x}_1(t-1)\ \ \ddot{x}_2(t-1)\cdots\ddot{x}_k(t-1)\ \ \ddot{x}_1(t-2)\ \ddot{x}_2(t-2)\cdots\ddot{x}_k(t-2)\cdots \\ &\cdots\ddot{x}_1(t-m)\ \ddot{x}_2(t-m)\cdots\ddot{x}_k(t-m)]\end{aligned} \tag{4.2.d}$$

$$\begin{aligned}\mathbf{F} = [&f_1(t)\ \ f_2(t)\cdots f_l(t)\ \ f_1(t-1)\ \ f_2(t-1)\cdots f_l(t-1)\cdots \\ &\cdots f_1(t-n)\ \ f_2(t-n)\cdots f_l(t-n)]\end{aligned} \tag{4.2.e}$$

The elements of $[W]$ and $[V]$ are w_{ij} and v_{ij}, respectively, and the elements of $\{q_w\}$ and $\{q_v\}$ are q_{wi} and q_{vi}. Carefully expanding equation (4.2.a) yields,

$$\begin{Bmatrix}\ddot{x}_1(t)\\ \ddot{x}_2(t)\\ \vdots\\ \ddot{x}_k(t)\end{Bmatrix} = \sum_{i=1}^{m}\hat{\mathbf{W}}_1^{(i)}\begin{Bmatrix}\ddot{x}_1(t-i)\\ \ddot{x}_2(t-i)\\ \vdots\\ \ddot{x}_k(t-i)\end{Bmatrix} + \sum_{j=0}^{n}\hat{\mathbf{W}}_2^{(j)}\begin{Bmatrix}f_1(t-j)\\ f_2(t-j)\\ \vdots\\ f_l(t-j)\end{Bmatrix} + \{C\} \tag{4.3.a}$$

where

$$\begin{bmatrix}\hat{\mathbf{W}}_1 & \hat{\mathbf{W}}_2\end{bmatrix} = [W][V] \tag{4.3.b}$$

$$\{C\} = [W]\{q_v\} + \{q_w\} \tag{4.3.c}$$

$$\hat{\mathbf{W}}_1 = [\hat{\mathbf{W}}_1^{(1)}\ \hat{\mathbf{W}}_1^{(2)} \cdots \hat{\mathbf{W}}_1^{(n)}] \tag{4.3.d}$$

$$\hat{\mathbf{W}}_2 = [\hat{\mathbf{W}}_2^{(0)}\ \hat{\mathbf{W}}_2^{(1)} \cdots \hat{\mathbf{W}}_2^{(m)}] \tag{4.3.e}$$

Equation (4.3.a) is similar to the time series model, ARX. The ARX model equates the equations of motion of a structural system. The dynamic characteristics of the system can be determined from the coefficient matrices of AR [92]. Note that, since the weight matrices of a trained ANN which has the topology shown in Figure 4.3 are later used for modal analysis, this kind of network was termed as modal analysis network (MAN for short) in the dissertation.

4.3.2 Estimation of Modal Parameters

After trained the MAN with the corresponding measurements, the modal parameters are extracted from the connective weights. Constructing the following transfer matrix,

$$[G] = \begin{bmatrix} 0 & \mathbf{I} & 0 & 0 & 0 \\ 0 & 0 & \mathbf{I} & 0 & 0 \\ \vdots & \vdots & \vdots & \vdots & \vdots \\ 0 & 0 & 0 & 0 & \mathbf{I} \\ \hat{\mathbf{W}}_1^{(n)} & \hat{\mathbf{W}}_1^{(n-1)} & \cdots & \hat{\mathbf{W}}_1^{(2)} & \hat{\mathbf{W}}_1^{(1)} \end{bmatrix} \tag{4.4}$$

enables the modal parameters to be determined from the eigenvalues and eigenvectors of it [93].

Let l_k and $\{y_k\}$ represent the kth eigenvalue and eigenvector of $[G]$, respectively. The eigenvalue, l_k, is normally a complex number, equal to $a_k + ib_k$.

The corresponding natural frequency and modal damping of the structural system are given by,

$$\tilde{g}_k = \sqrt{s_k^2 + g_k^2} \tag{4.5}$$

$$x_k = -s_k / \tilde{g}_k \tag{4.6}$$

where $\tilde{g}_k$ is the pseudo-undamped circular natural frequency; x_k is the modal damping ratio;

$$g_k = \frac{1}{\Delta t}\tan^{-1}\left(\frac{b_k}{a_k}\right) \tag{4.7}$$

$$s_k = \frac{1}{2\Delta t}\ln(a_k^2 + b_k^2) \tag{4.8}$$

and $\frac{1}{\Delta t}$ is the sampling rate of measurement.

The special composition of $[G]$ in equation (4.4) yields the following property of its eigenvectors.

$$\{y_k\} = (\{y_k\}_1^T, l_k\{y_k\}_1^T, l_k^2\{y_k\}_1^T, ..., l_k^{n-1}\{y_k\}_1^T)^T \tag{4.9}$$

where $\{y_k\}_1$ is the complex modal shape of the system, corresponding to the natural frequency, $\tilde{g}_k$.

Notably, the formulation shown above is easily extended to cases with multiple hidden layers, by modifying only the definitions for $\hat{\mathbf{W}}_1^{(i)}$, $\hat{\mathbf{W}}_2^{(j)}$, and $\{C\}$ in equation (4.3).

Figure 4.4 give a summarized view on the operation procedure of the ANNSI model.

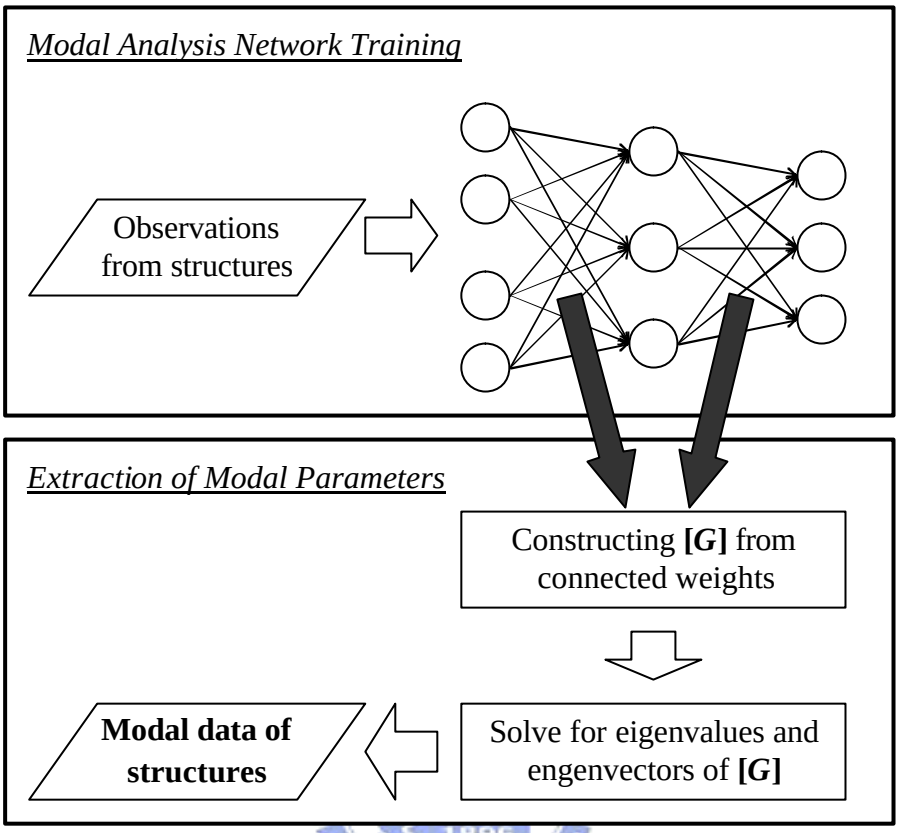

Figure 4.4 Operation procedure of the ANNSI model

Various neural networks with the architecture given in Figure 4.3 (i.e. modal analysis networks, MANs), can be established, from the measured responses of a structure in earthquakes with various magnitudes. The modal parameters for the structure in different earthquakes can be determined from the established MANs, by the above approach. Considerable changes in modal parameters, corresponding to different MANs, indicate significant changes in the structural properties in different earthquakes.

4.3.3 Example－ Modal Analysis of a Five-Story Steel Frame in NCREE

This example is a dynamic test of a five-story steel frame on the shaking table (Figure 4.5) conducted in National Center for Research on Earthquake Engineering (NCREE) in Taiwan. Shaking table tests are often performed in a laboratory to examine the behavior of structures in earthquakes. The NCREE in Taiwan undertook a series of shaking table tests on a 3 m long, 2 m wide, and 6.5 m high steel frame [94] to generate a set of earthquake response data for this benchmark model of a five-story steel structure. Lead blocks were piled on each floor such that the mass of each floor was approximately 3664 kg. The frames were subjected to the base excitation of the Kobe earthquake, weakened by various levels. The displacement, velocity, and acceleration response histories of each floor were recorded during the shaking table tests. Additionally, some strain gauges were also installed in one of the columns and near the first floor. The sampling rate of the raw data was 1000 Hz. These raw data were reproduced with a 200 Hz sampling rate by taking one data point out of every five raw data points to save computational time and to match to the typical sampling rate for real applications.

Notably, it was reported [94] that the frame responded linearly when it subjected to 8%, 10%, 20%, 40%, and 52% of the strength of the Kobe earthquake. Measured strains and visual inspection revealed that 60% of the strength of the Kobe earthquake input caused the steel columns near the first floor to yield. In the following, only the responses and inputs in the long span direction are discussed.

Figure 4.5 A photo of the five-story steel frame in NCREE

Figure 4.6 depicts time histories of the acceleration responses of each floor, when the steel frame was subjected to 8% of the strength of the Kobe earthquake. The steel frame responded linearly at this level. The large responses between 4.5 and 12.5 seconds were used to train an ANN and thus, to some extent, reduce the noise effect. The architecture of the ANN is as shown in Figure 4.3, with k=5, l=1, m=n=30 and ten

nodes in the hidden layer. This architecture was used throughout this example. The acceleration responses of each floor relative to the base were used to train an MAN. Figure 4.7 shows the excellent correspondence between the observed responses and the computed responses from the trained MAN for all floors. It is noted that the computed responses in Figure 4.7 were obtained from the trained MAN by using the observed data as input of the MAN.

Evaluation of the Correlation of Modal Shapes

An index commonly used to evaluate the correlation of modal shapes is based on the modal assurance criterion (*MAC*) defined as [95],

$$MAC(\mathbf{f}_{iR},\mathbf{f}_{iC}) = \frac{\left|\mathbf{f}_{iR}^{T}\mathbf{f}_{iC}^{*}\right|^{2}}{\mathbf{f}_{iR}^{T}\mathbf{f}_{iR}^{*}\,\mathbf{f}_{iC}^{T}\mathbf{f}_{iC}^{*}} \tag{4.10}$$

where * denotes the complex conjugate, $\mathbf{f}_{iR}$ and $\mathbf{f}_{iC}$ represent the ith complex mode shapes for the reference state and the current state to which it is to be compared, respectively. Apparently, two corresponding modes are highly correlated if the *MAC* value is close to one, and uncorrelated if it is near zero.

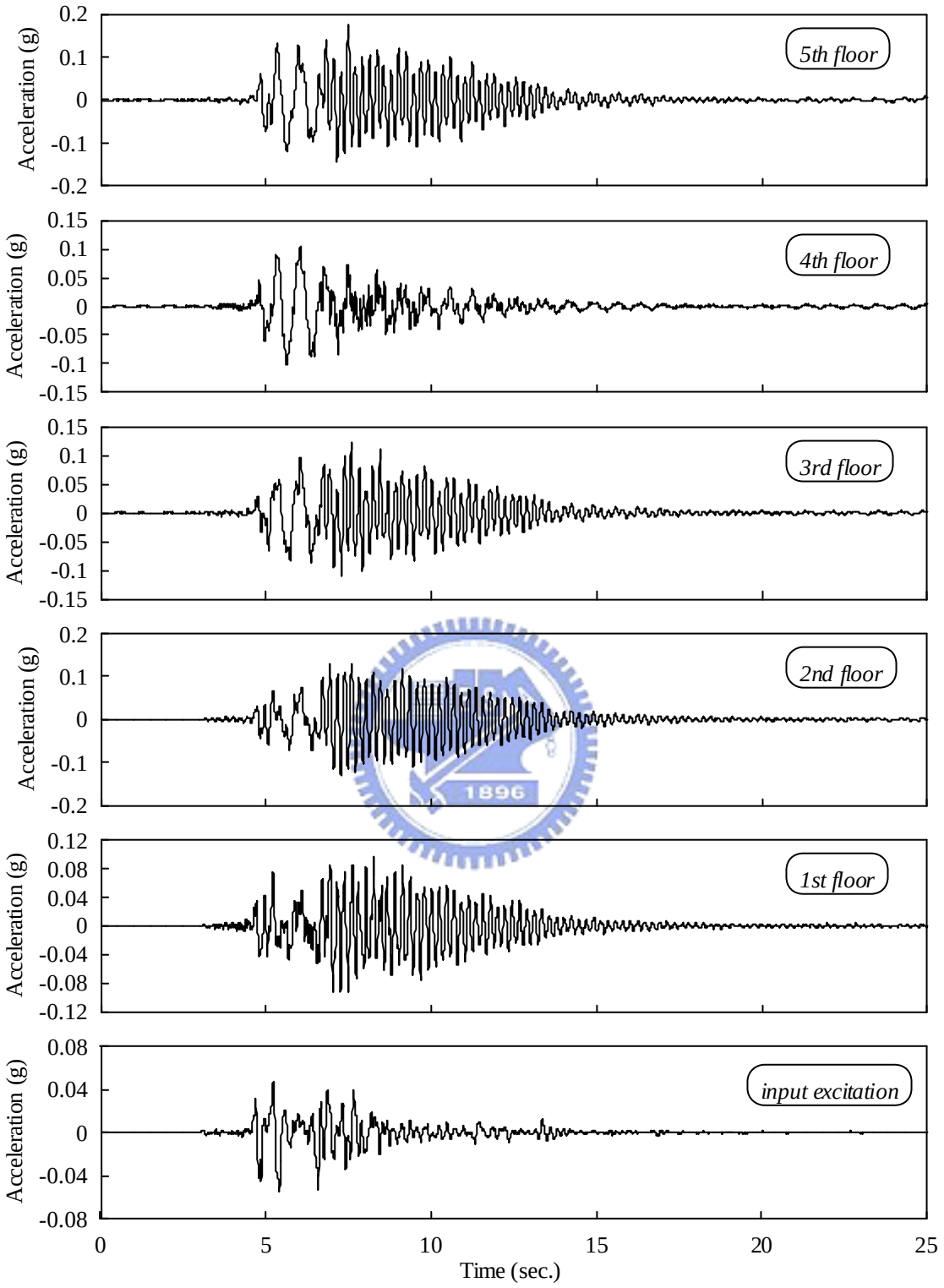

Figure 4.6 Response histories for 8% Kobe earthquake input

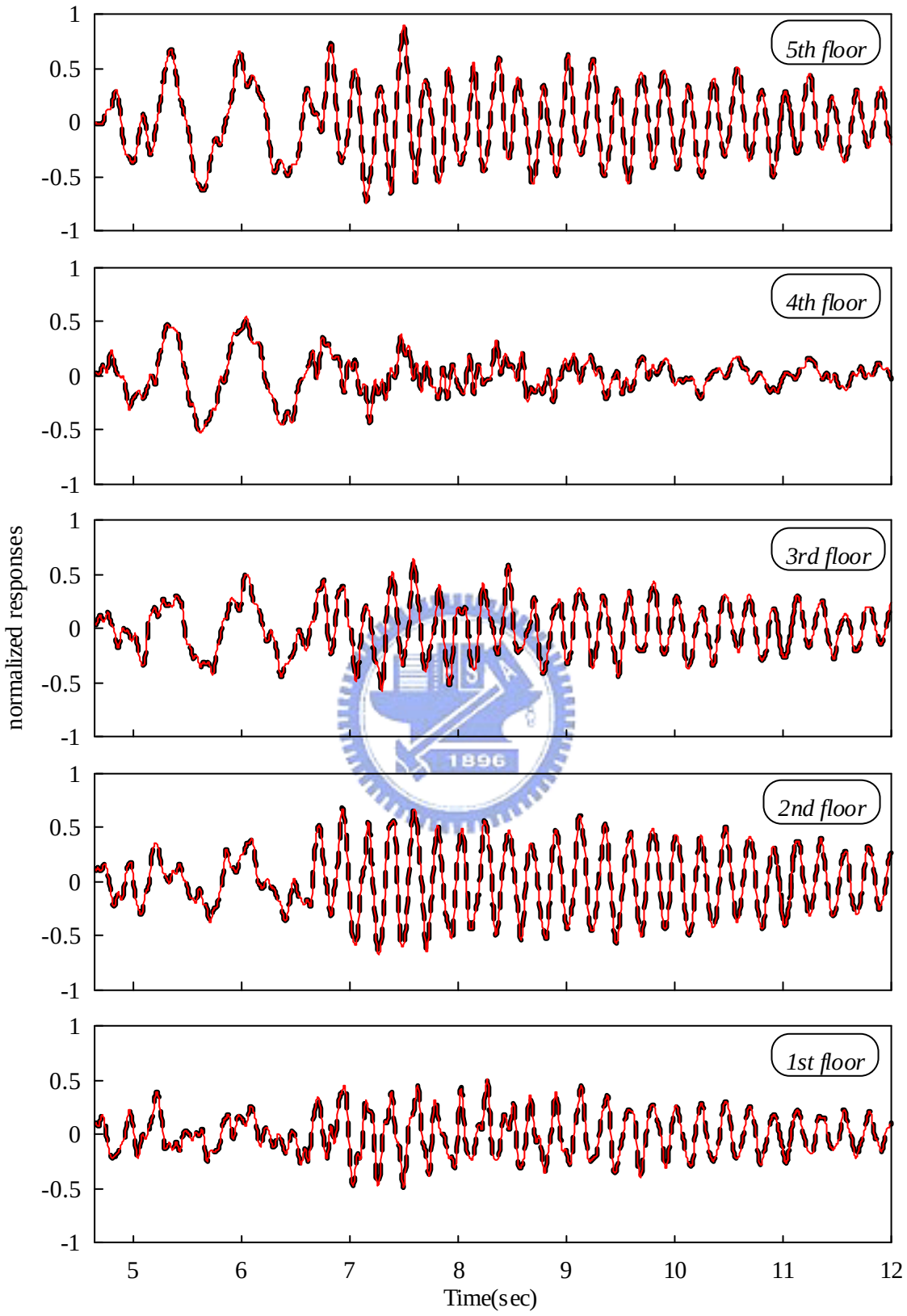

Figure 4.7 Comparison between the measured (solid line) and predicted (dash line) responses for 8% Kobe earthquake input.

As will show later, the *MAC* value is not very sensitive to the changes in modal shapes for the cases considered in the example. Thus, an index proposed by Trifunac [96] for modal shapes in a proportional damping system, is also used for evaluating the identification results. The index is defined as,

$$e = \left(\frac{(\mathbf{f}_{iR} - a\mathbf{f}_{iC})^T (\mathbf{f}_{iR} - a\mathbf{f}_{iC})^*}{\mathbf{f}_{iR}^T \mathbf{f}_{iR}^*}\right)^{1/2} \tag{4.11}$$

where the complex constant, a, is obtained by minimizing $(\mathbf{f}_{iR} - a\mathbf{f}_{iC})^T (\mathbf{f}_{iR} - a\mathbf{f}_{iC})^*$. Equation (4.11) reveals that e is close to zero when the two modal shapes are highly correlated.

Identified Results and Discussions

Table 4.1 lists the identified modal parameters obtained from the trained MAN, which excellently agree with those obtained by Huang and Lin [97] who used a subspace technique to process the same response data. This consistency confirms the correctness of the proposed procedure of determining the modal parameters from an ANN.

The measured acceleration responses of the frame under the base excitations with various reduction levels of the Kobe earthquake, enables the corresponding ANNs to be established and the corresponding modal parameters to be determined. Table 4.2 summarizes the results, in which the values, *MAC* and *e*, designate the correlation between the modal shapes for an input of 20% Kobe earthquake and those for inputs with other reduction levels.

Table 4.1 Identified modal parameters for 8% Kobe earthquake input.

Method	Mode	Frequency (Hz)	Damping (%)	MAC	*e* (%)
ANNSI	**1**	1.40	1.56	1.00	0.38
	2	4.53	0.17	1.00	0.15
	3	8.23	0.17	1.00	0.31
	4	12.39	0.13	1.00	0.47
	5	15.99	0.11	1.00	0.47
subspace [97]	**1**	1.40	1.30	/	/
	2	4.53	0.16	/	/
	3	8.23	0.19	/	/
	4	12.39	0.13	/	/
	5	15.99	0.10	/	/

Note: / : no data available

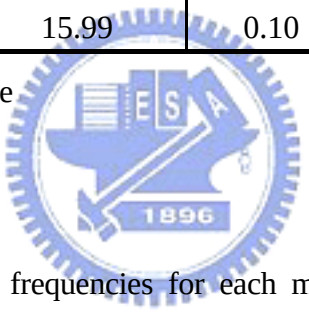

Table 4.2 reveals that the frequencies for each mode generally decrease as the excitation magnitude increases, but the changes in frequency are quite small. Generally, the modal damping values increase with excitation magnitude. The modal damping values for the 60% Kobe earthquake are much greater than those for the 10% Kobe. Interestingly, only the damping for the first mode exceeds 1% while the damping for the other modes is typically much less than 1%. The *MAC* values in Table 4.2 indicate that the modal shapes for the 20% Kobe earthquake are likely to correlate closely with those for other excitations. However, *e* values clearly show that the modal shapes of the higher modes (3rd to 5th) for the 60% Kobe earthquake notably differ from those for the 20% Kobe earthquake, since the corresponding *e* values exceed 10%. Apparently, the *e* values are more sensitive to the differences in modal shapes than the

MAC values. The damping and *e* values truly reflect the fact of possible damage of the frame under the 60% Kobe earthquake input.

Table 4.2 Identified modal parameters for different inputs.

Excitation	Mode	Frequency (Hz)	Damping (%)	MAC	*e* (%)
10% Kobe	**1**	1.40	1.65	1.00	1.00
	2	4.53	0.18	1.00	0.59
	3	8.24	0.22	1.00	0.66
	4	12.38	0.16	1.00	0.79
	5	16.00	0.16	1.00	1.17
20% Kobe	**1**	1.39	1.73	/	/
	2	4.53	0.25	/	/
	3	8.23	0.28	/	/
	4	12.37	0.18	/	/
	5	15.97	0.15	/	/
40% Kobe	**1**	1.38	2.42	1.00	0.65
	2	4.50	0.47	1.00	0.92
	3	8.18	0.19	1.00	2.26
	4	12.36	0.21	1.00	6.58
	5	15.93	0.07	1.00	4.54
52% Kobe	**1**	1.37	2.89	1.00	0.42
	2	4.49	0.69	1.00	1.13
	3	8.14	0.53	1.00	3.36
	4	12.33	0.15	1.00	5.48
	5	15.91	0.58	1.00	6.83
60% Kobe	**1**	1.35	3.73	1.00	2.21
	2	4.45	0.92	1.00	5.24
	3	8.07	0.84	0.99	11.52
	4	12.24	0.83	0.98	13.42
	5	15.88	0.26	0.98	13.13

Note: / : no data available

4.4 Identification Of Strain Mode Shapes

The theories as well as the practical applications of modal analysis using displacement, velocity, and acceleration information had been extensively developed. Moreover, most of the studies of experimental modal analysis employ displacement, velocity, and acceleration observations from a structural system for the purpose of system identification. However, seldom studies employ the strain information for modal analysis of the structures. As an important and sensitive feature in the damage detection of structures in this research, the structural strain responses are measured and analyzed to be a basis for monitoring the condition of structures. As well, the strain mode shapes are extracted from the strain measurements to be a suitable damage indicator for detecting the structural damage.

Basing on the ANNSI model, the approach for obtaining the strain mode shapes is introduced in this section. Before that, the theoretical basis of the approach is first presented.

4.4.1 Equation of Strain Motion of a System

For a finite element, the displacement $\{u\}$ at any point within the element can be expressed by

$$\{u\} = \mathbf{N}\{x\} \tag{4.12}$$

in which $\mathbf{N}$ is predefined shape function matrix and $\{x\}$ represents a listing of nodal displacements for a particular element.

With displacements known at all points within the element the strains at any point

can be determined by the following relationship:

$$\{e\} = \mathbf{S}\{u\} \tag{4.13}$$

where **S** is a suitable linear operator. Substitute equation (4.12) for $\{u\}$, the above equation can be rewritten as

$$\{e\} = \mathbf{SN}\{x\} = \mathbf{B}\{x\} \tag{4.14}$$

which makes

$$\{x\} = \mathbf{B}^{-1}\{e\} \tag{4.15}$$

where **B** is the strain-nodal displacement matrix of the element.

When the finite elements of the dynamic system were assembled to the equation of motion which yields

$$\mathbf{M}\{\ddot{x}\} + \mathbf{C}\{\dot{x}\} + \mathbf{K}\{x\} = \{f\} \tag{4.16}$$

in which **M**, **C**, and **K** are the system mass, damping, and stiffness matrices, respectively; the components in $\{x\}$ and $\{f\}$ are the nodal displacements and external forces, respectively.

Using equation (4.15), since **B** is independent of time the following relationships hold.

$$\{\ddot{x}\} = \mathbf{B}^{-1}\{\ddot{e}\} \tag{4.17.a}$$

$$\{\dot{x}\} = \mathbf{B}^{-1}\{\dot{e}\} \tag{4.17.b}$$

Impose equations (4.15) and (4.17) on equation (4.16), the equation of motion using notations of strain is derived.

$$\overline{\mathbf{M}}\{\ddot{e}\} + \overline{\mathbf{C}}\{\dot{e}\} + \overline{\mathbf{K}}\{e\} = \{f\} \tag{4.18.a}$$

with

$$\overline{\mathbf{M}} = \mathbf{M}\mathbf{B}^{-1}; \tag{4.18.b}$$

$$\overline{\mathbf{C}} = \mathbf{C}\mathbf{B}^{-1}; \text{ and} \tag{4.18.c}$$

$$\overline{\mathbf{K}} = \mathbf{K}\mathbf{B}^{-1} \tag{4.18.d}$$

It is evidently seen that, this equation has the same form to equation (4.16) except for the notation of acceleration was replaced by strain. Therefore, the ANNSI model can be applied to the strain measurements. Notably, the identified mode shapes are the strain mode shapes of the system.

4.4.2 Relationship between Strain and Displacement Modal parameters

As known, the eigenvalues and eigenvectors of equation (4.16) can be solved by

$$[\mathbf{K} - w_n^2\mathbf{M}]f_n = 0 \tag{4.19}$$

where w_n^2 and f_n represent the nth natural frequency and displacement mode shape of the system. Expanding the above equation leads to

$$\mathbf{K}f_n = w_n^2\mathbf{M}f_n \tag{4.20}$$

Pre-multiplying it with $\mathbf{M}^{-1}$ yields

$$\mathbf{M}^{-1}\mathbf{K}f_n = w_n^2 f_n \tag{4.21}$$

Likewise, the eigenvalues and eigenvectors of equation (4.18.a) can be solved by

$$[\overline{\mathbf{K}} - w_n^2 \overline{\mathbf{M}}]\tilde{f}_n = 0 \tag{4.22}$$

where $\tilde{f}_n$ represent the *n*th strain mode shape of the system. Expanding the above equation leads to

$$\overline{\mathbf{K}}\tilde{f}_n = w_n^2 \overline{\mathbf{M}}\tilde{f}_n \tag{4.23}$$

Pre-multiplying it with $\overline{\mathbf{M}}^{-1}$ yields

$$\overline{\mathbf{M}}^{-1}\overline{\mathbf{K}}\tilde{f}_n = w_n^2 \tilde{f}_n \tag{4.24}$$

Using equations (4.18.b) to (4.18.d), the above equation becomes

$$\mathbf{B}\mathbf{M}^{-1}\mathbf{K}\mathbf{B}^{-1}\tilde{f}_n = w_n^2 \tilde{f}_n \tag{4.25}$$

Further pre-multiplying it with $\mathbf{B}^{-1}$ results in

$$\mathbf{M}^{-1}\mathbf{K}\mathbf{B}^{-1}\tilde{f}_n = w_n^2 \mathbf{B}^{-1}\tilde{f}_n \tag{4.26}$$

Compare equation (4.26) with equation (4.21), the relationship between the displacement mode shape and strain mode shape can be found which is

$$\mathbf{B}^{-1}\tilde{f}_n = f_n \quad \text{or} \quad \tilde{f}_n = \mathbf{B} f_n \tag{4.27}$$

Subsequently, the relationship between the strain and displacement modal damping is investigated. Let the damping matrix **C** in equation (4.16) to be proportional damping which is

$$\mathbf{C} = a\mathbf{M} + b\mathbf{K} \tag{4.28}$$

where *a* and *b* are constants. Since the system matrices, **M**, **C**, and **K** can be

simultaneously diagonalized by equivalence transformation using the orthogonal eigenvector matrix, $\Phi = [f_1\ f_2 \cdots f_n]$. Equation (4.28) is diagonalized in the following form:

$$\Phi^T \mathbf{C} \Phi = a\Phi^T \mathbf{M} \Phi + b\Phi^T \mathbf{K} \Phi \tag{4.29.a}$$

with

$$\Phi^T \mathbf{C} \Phi = diag[C_n] = diag[2x_n w_n M_n] \tag{4.29.b}$$

$$\Phi^T \mathbf{M} \Phi = diag[M_n] \tag{4.29.c}$$

$$\Phi^T \mathbf{K} \Phi = diag[K_n] = diag[w_n^2 M_n] \tag{4.29.d}$$

where C_n, M_n, and K_n are the nth modal damping, modal mass, and modal stiffness, respectively. Then the displacement modal damping ratios for each mode are calculated from the decoupled equation.

Since the system matrices in equation (4.18.a) lack any specific symmetry, the system which is described by equation (4.18.a) is termed as nonclassical dynamic system. The eigenvalue problem associated with this equation is

$$(l^2 \overline{\mathbf{M}} + l\,\overline{\mathbf{C}} + \mathbf{K})\{q\} = 0 \tag{4.30}$$

where l is a complex number and $\{q\}$ is a constant column vector. Further rewrite this equation as

$$(l^2 \mathbf{I} + l\,\overline{\mathbf{M}}^{-1}\overline{\mathbf{C}} + \overline{\mathbf{M}}^{-1}\mathbf{K})\{q\} = 0 \tag{4.31}$$

which necessarily has the same eigenvalues as equation (4.30).

If equation (4.28) is back-multiplied by $\mathbf{B}^{-1}$, it becomes

$$\overline{\mathbf{C}} = a\overline{\mathbf{M}} + b\overline{\mathbf{K}} \tag{4.32}$$

According to this equation, the strain damping matrix $\overline{\mathbf{C}}$ remains proportional. Therefore, equation (4.31) can be transformed into a equivalent symmetric system by an eigenvalue preserving transformation [98]. The transformations of the asymmetric matrices, $\overline{\mathbf{M}}^{-1}\overline{\mathbf{C}}$ and $\overline{\mathbf{M}}^{-1}\overline{\mathbf{K}}$, are

$$\overline{\mathbf{M}}^{-1}\overline{\mathbf{C}} = \mathbf{B}\mathbf{B}^T(\overline{\mathbf{M}}^{-1}\overline{\mathbf{C}})(\mathbf{B}^{-1})^T\mathbf{B}^{-1} \tag{4.33.a}$$

$$\overline{\mathbf{M}}^{-1}\overline{\mathbf{K}} = \mathbf{B}\mathbf{B}^T(\overline{\mathbf{M}}^{-1}\overline{\mathbf{K}})(\mathbf{B}^{-1})^T\mathbf{B}^{-1} \tag{4.33.b}$$

More details about how the transformation is implemented can be seen in the reference [98]. This result provides a necessary and sufficient condition for the existence of a linear transformation that transforms equation (4.31) into an equivalent symmetric system. When this condition is satisfied by a given system, the dynamics of the system can be described in terms of the well-developed theory for the damped symmetric systems. Moreover, the damping of the system can be evaluated from the equivalent symmetric system. However, due to the unknown $\mathbf{B}$ matrix, the relationship between the strain and displacement modal damping ratios is not directly established herein. Since the strain modal damping ratio is not the key data that used for structural health monitoring, the idea of the relationship is only introduced.

4.5 System Monitoring Networks

In general, the system identification methods can be classified into two major categories, which are parametric and nonparametric, according to their identified results. Most ANN-based methods belong to the latter one owing to the feature of

'black box'. Nevertheless, the ANNSI model is parametric since it can produce the physical parameters of a structural system. In addition to the parametric ANNSI model, the ways of nonparametric identification are investigated in this research and presented in this section. Two system-identification-based health monitoring networks are proposed herein. They are global monitoring networks and decentralized monitoring networks.

4.5.1 Global Monitoring Networks

Marsi *et al*. [11] proposed an important idea for the health monitoring of structural damage using neural networks. They presented an ANN-based approach for the detection of changes in the structural characteristics of unknown systems. The major contribution of their work is that the proposed approach does not need a priori information about the nature of the system which is usually difficult to obtain in real-world situations. The damage detection procedure of this methodology, which is depicted in Figure 4.8, is divided into two steps: (1) the training of the identification network and (2) the detection of structural damage using the trained network.

In the training stage, as shown in the top of Figure 4.8, a neural network is trained by the vibration measurements obtained from a healthy structure. In the damage detection stage, as shown in the bottom of Figure 4.8, the trained network is fed with comparably vibration measurements from the same structure under different episodes of response in order to monitor the condition of the structure.

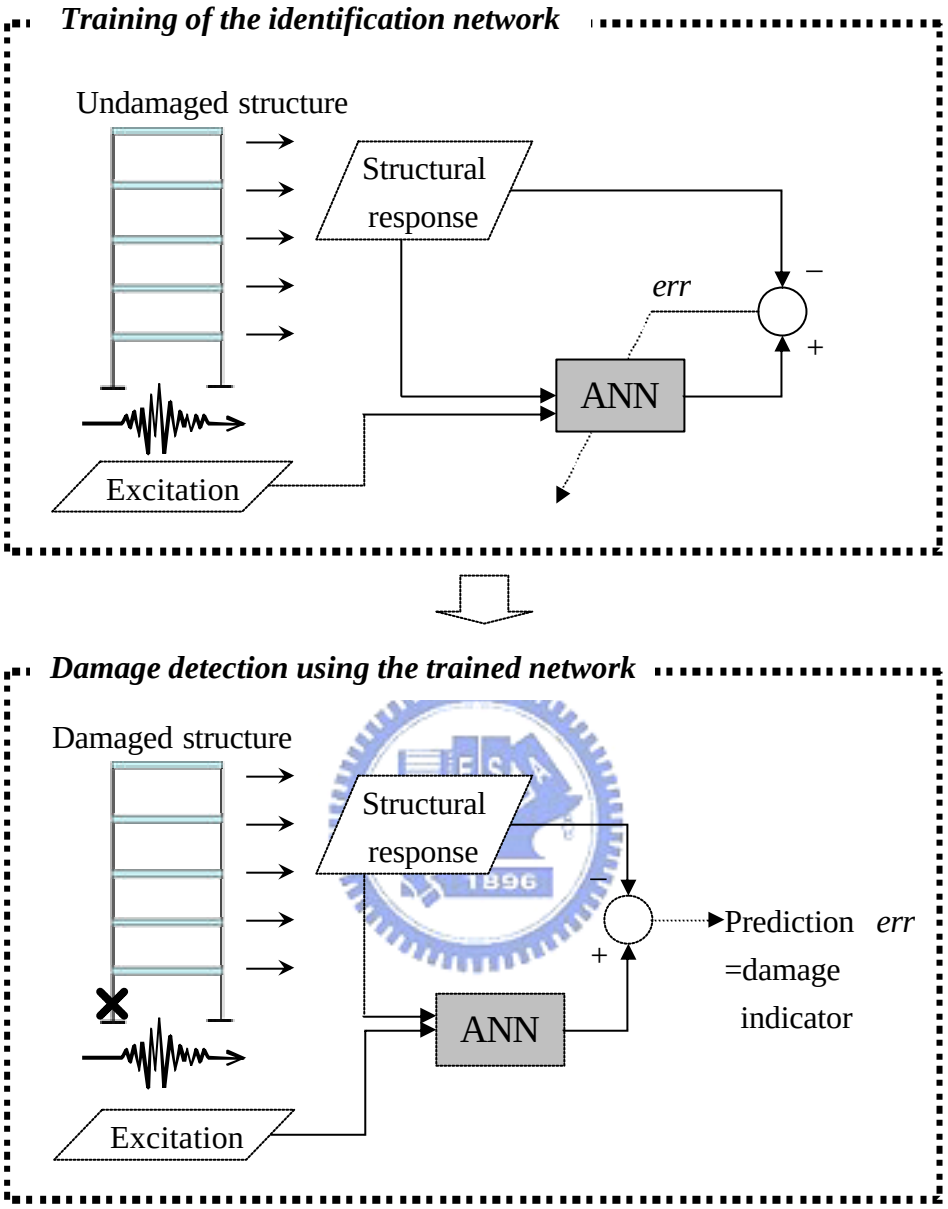

Figure 4.8 Schematic diagram of health monitoring using neural networks

According to the input variables of the MAN (Figure 4.3), it is found that the network provide a global view on the target structure since it is trained by the system input excitation and the structural responses at most DOFs. Therefore, if the networks that similar to MAN are employed for the health monitoring of structures, they are

generally called global monitoring networks.

4.5.2 Decentralized Monitoring Networks

Nakamura *et al*. [12] further applied the methodology proposed by Marsi *et al*. [11] to the actual data obtained from ambient vibration measurements on a steel building structure that was damaged under strong seismic motion. In their study, an individual network was prepared for each story and each network represents a physical system corresponding to a specific story of the building. Obviously, such networks provide a local view on the structure; as a result, they are generally called decentralized monitoring networks.

Although the presented methodology by Nakamura *et al*. had successfully identified the difference between the damaged and undamaged stories, the methodology is limited due to the data needed for training the neural networks. The formulation they proposed must adopt the velocity and displacement information while displacement is usually difficult to be measured in practical situations. Furthermore, the instrumentation was selected to directly measure velocity. Since the acceleration and displacement data are needed, they were computed by differentiation or integration with respect to time. Therefore, errors arose in the computations of differentiation and integration. Furthermore, the interstory restoring force was extracted by cumulatively summing up the inertia force at each floor from the top of the building down to the basement. Accordingly, structural response at every story should be measured which is usually not possible for a large structure however.

Accordingly, an approach based on the concept of decentralized monitoring

networks is presented herein. Only measured acceleration data are needed in this approach.

For an *n*-DOFs dynamic system, the motion of equation is

$$\mathbf{M}\{\ddot{x}(t)\} + \mathbf{C}\{\dot{x}(t)\} + \mathbf{K}\{x(t)\} = -\mathbf{M}\{\mathbf{1}\}\ddot{u}_g(t) \tag{4.33}$$

If the system is assumed to be a shear frame structure and the damping matrix is assumed to be proportional damping, the extended form of equation (4.33) is

$$\mathbf{M}\begin{Bmatrix} \ddot{x}_1(t) \\ \ddot{x}_2(t) \\ \vdots \\ \ddot{x}_n(t) \end{Bmatrix} + \mathbf{C}\begin{Bmatrix} \dot{x}_1(t) \\ \dot{x}_2(t) \\ \vdots \\ \dot{x}_n(t) \end{Bmatrix} + \mathbf{K}\begin{Bmatrix} x_1(t) \\ x_2(t) \\ \vdots \\ x_n(t) \end{Bmatrix} = -\begin{Bmatrix} m_1 \\ m_2 \\ \vdots \\ m_n \end{Bmatrix}\ddot{u}_g(t) \tag{4.34.a}$$

where

$$\mathbf{M} = \begin{bmatrix} m_1 & 0 & \cdots & 0 \\ 0 & m_2 & & \vdots \\ \vdots & & \ddots & 0 \\ 0 & \cdots & 0 & m_n \end{bmatrix} \tag{4.34.b}$$

$$\mathbf{C} = \begin{bmatrix} c_{11} & c_{12} & 0 & \cdots & \cdots & 0 \\ c_{21} & c_{22} & c_{23} & & & \vdots \\ 0 & c_{32} & c_{33} & & & \vdots \\ \vdots & & & \ddots & c_{(n-2)(n-1)} & 0 \\ \vdots & & & c_{(n-1)(n-2)} & c_{(n-1)(n-1)} & c_{(n-1)n} \\ 0 & \cdots & \cdots & 0 & c_{n(n-1)} & c_{nn} \end{bmatrix} \tag{4.34.c}$$

$$\mathbf{K} = \begin{bmatrix} k_1+k_2 & -k_2 & 0 & \cdots & \cdots & 0 \\ -k_2 & k_2+k_3 & -k_3 & & & \vdots \\ 0 & -k_3 & k_3+k_4 & & & \vdots \\ \vdots & & & \ddots & -k_{(n-1)} & 0 \\ \vdots & & & -k_{(n-1)} & k_{(n-1)}+k_n & -k_n \\ 0 & \cdots & \cdots & 0 & -k_n & k_n \end{bmatrix} \tag{4.34.d}$$

Expanding equation (4.34.a) enables *n* equations to be obtained. For explanation, now take the first two equations to be considered and then transform them to the discrete forms.

$$m_1\ddot{x}_1[i]+c_{11}\dot{x}_1[i]+c_{12}\dot{x}_2[i]+(k_1+k_2)x_1[i]-k_2x_2[i]=-m_1\ddot{u}_g[i] \tag{4.35.a}$$

$$\begin{aligned} m_2\ddot{x}_2[i]+c_{21}\dot{x}_1[i]+c_{22}\dot{x}_2[i]+c_{23}\dot{x}_3[i]-k_2x_1[i] \\ +(k_2+k_3)x_2[i]-k_3x_3[i]=-m_2\ddot{u}_g[i] \end{aligned} \tag{4.35.b}$$

where $\ddot{x}[i]$, $\dot{x}[i]$, and $x[i]$ are the structural acceleration, velocity, and displacement at the *i*th time step, respectively.

Suppose the velocity and displacement at current time step are correlated with the previous input excitation and structural response information. The formulations of velocity and displacement can be defined as

$$\dot{x}_j[i]=F_j(\ddot{x}_j[i-1],\ddot{x}_j[i-2],\ldots,\ddot{x}_j[i-p_1],\ddot{u}_g[i],\ddot{u}_g[i-1],\ldots,\ddot{u}_g[i-p_2]) \tag{4.36.a}$$

$$x_j[i]=G_j(\ddot{x}_j[i-1],\ddot{x}_j[i-2],\ldots,\ddot{x}_j[i-q_1],\ddot{u}_g[i],\ddot{u}_g[i-1],\ldots,\ddot{u}_g[i-q_2]) \tag{4.36.b}$$

where *F* and *G* represent the functional mappings; *p* and *q* are the number of previous time steps should be involved to calculate the velocity and displacement responses at the current time step.

Imposing equation (4.36) on equation (4.35) by setting *j* equal to 1, 2, and 3, respectively, equation (4.35) becomes

$$m_1\ddot{x}_1^{\,a}[i]=-c_{11}F_1-c_{12}F_2-(k_1+k_2)G_1+k_2G_2 \tag{4.37.a}$$

$$m_2\ddot{x}_2^{\,a}[k]=-c_{21}F_1-c_{22}F_2-c_{23}F_3+k_2G_1-(k_2+k_3)G_2+k_3G_3 \tag{4.37.b}$$

where $\ddot{x}^a[i] = \ddot{x}[i] + \ddot{u}_g[i]$ is the measured absolute acceleration. Likewise, the rest equations from expanding equation (4.34.a) can be derived to the similar form as equation (4.37).

Equation (4.37) shows that the absolute acceleration response at current time is a function of the damping and stiffness which adjacent to the DOF of interest and the responses in previous time steps. Since neural networks can be used for system identification purposes, two neural networks, named Net_1 and Net_2, are employed to learn the relationships in equations (4.37.a) and (4.37.b), respectively. Again, one can use neural networks to identify each of the rest expanded equations of equation (4.34.a).

For the damage detection purpose, the procedure shown in Figure 4.8 is utilized for each network Net_s (s=1~n). Refer to equation (4.37), if the column at 1st story was damaged (i.e. k_1 changed), the relationship where the term k_1 existed in alter (i.e. equation (4.37.a)), which causes the increment in prediction error from Net_1 but not from other networks. Likewise, if the column at 2nd story was damaged (i.e. k_2 changed), the prediction errors from Net_1 and Net_2 increase, but that from others don't. For other damage cases, the networks of which the predicted output errors increase can be easily obtained in the same way. As a result, the performance of the network Net_s exhibits the following properties:

(1) If no damage occurs in any structural element, the predicted outputs from Net_s will close to the measured responses.

(2) If stiffness reduction occurred in k_i, the predicted output errors from $Net_{(i-1)}$ and Net_i will then increase, and the prediction errors from the rest networks

won't. Restated, if the prediction error from Net_i increase, that means k_i or $k_{(i+1)}$ may be damaged.

According to the aforementioned properties, the decentralized monitoring networks can be used to identify damage location in simple way.

4.5.3 Example 1— Health Monitoring of a Five-Story Steel Frame Using Global Monitoring Networks

Following the example in section 4.3.3, this example employs the trained MAN as global monitoring network to monitor the structural response in different earthquake events. The MAN is expected to be able to predict accurately the current responses, from previously measured responses and inputs, if the structural system remains linear and the modal properties do not significantly change. However, when the structural system is damaged or has deteriorated, it will exhibit nonlinear behavior resulting in a large error in the responses of this damaged structure, predicted by the trained MAN for the healthy, linear structure. The indexes proposed by Masri *et al*. [66] can be used to quantify this error. However, for simplicity in this example, only the mean absolute error (*MAE*) between the output predicted by the trained ANN, and the measured acceleration responses is computed for each DOF, and is defined as,

$$MAE(i) = \frac{1}{T}\sum_{t=1}^{T}\left|y_{im}(t) - y_{ip}(t)\right| \tag{4.38}$$

where i represents the ith DOF, and y_{im} and y_{ip} are the normalized measurements and the predicted responses for the ith DOF, respectively.

The responses at a moderate reduction level (say, 20%) of the Kobe earthquake

input were selected to establish the MAN to predict the responses to other inputs (i.e. 10%, 40%, 52%, and 60% Kobe earthquake). The *MAE* values of each floor for various reduction levels of the Kobe earthquake are divided by the *MAE* value for the 20% Kobe earthquake and presented in Figure 4.9. The small changes in the modal parameters for the frame with different inputs, discussed in the section 4.3.3, cause the prediction errors to increase for the 10%, 40% and 52% Kobe earthquake inputs. The relative *MAE* values for the responses to the 60% Kobe earthquake input greatly exceed the other relative *MAE* values, confirming the reported nonlinear responses to the 60% Kobe earthquake input [94]. As mentioned, MAN provides a global view on the structure been monitored, therefore further investigation is required to determine whether the larger relative *MAE* values for the first and second floors in the 60% Kobe earthquake input follow from the yielding of the columns near the first floor.

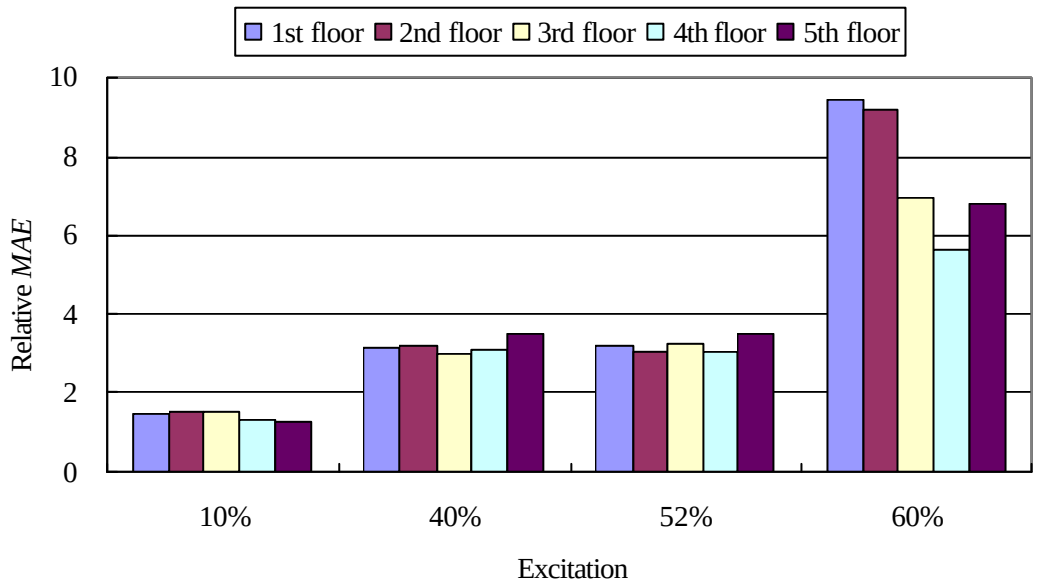

Figure 4.9 Relative mean absolute errors of predictions for the Kobe Earthquake inputs with various reduction levels

4.5.4 Example 2－ Damage Detection of a Six-Story Steel Frame Using Decentralized Monitoring Networks

A numerical example of a six-story shear frame structure is presented to investigate the capabilities of decentralized monitoring network. The model of the six-story building structure is shown in Figure 4.10. The structural acceleration response is calculated with the El-Centro earthquake inputs via the state space procedure. In this example, the damage scenarios are simulated by the reduction of story stiffness. Five damage cases which are shown in Table 4.3 are discussed. Notably, the symbols Dam_k_i ($i = 1 \sim 3$) in Table 4.3 denote that the damage results in reduction of stiffness of k_i in single site. Similarly, the symbols $Dam\_k_i \& k_j$ ($i \neq j$) mean that the damage results in reduction of stiffness of k_i and k_j in multiple sites.

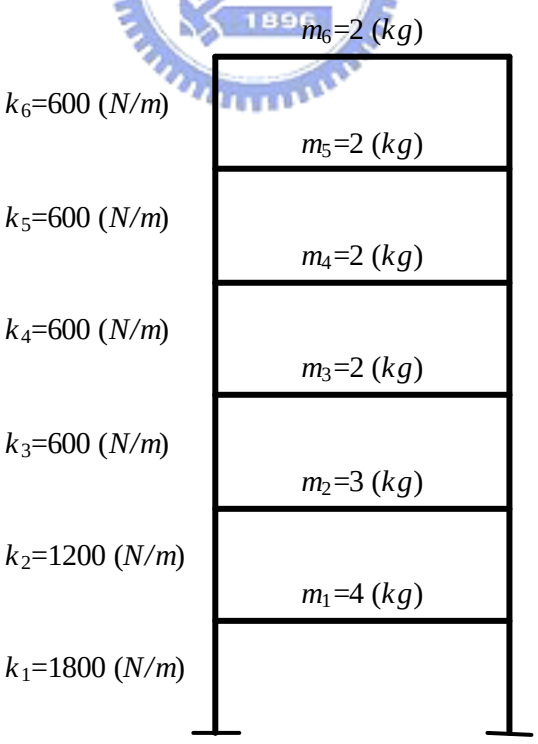

Figure 4.10 Model of a six-story shear frame structure

Table 4.3 Damage cases under discussion

No	Damage class	Damage level
Case 1	Dam_k_1	20%
Case 2	Dam_k_2	20%
Case 3	Dam_k_3	20%
Case 4	$Dam\_k_1 \& k_2$	10%&10%
Case 5	$Dam\_k_1 \& k_3$	10%&10%

Suppose the acceleration responses of all DOFs are measured and hence six decentralized monitoring networks (Net_i, i=1~6) are trained based on the relationship of equation (4.37). For example, Net_1 is used to monitor the 1st DOF of the structure using the relationship of equation (4.37.a). The topology of Net_1 is shown in Figure 4.11. The decentralized monitoring networks for monitoring other DOFs can be organized and trained in similar way.

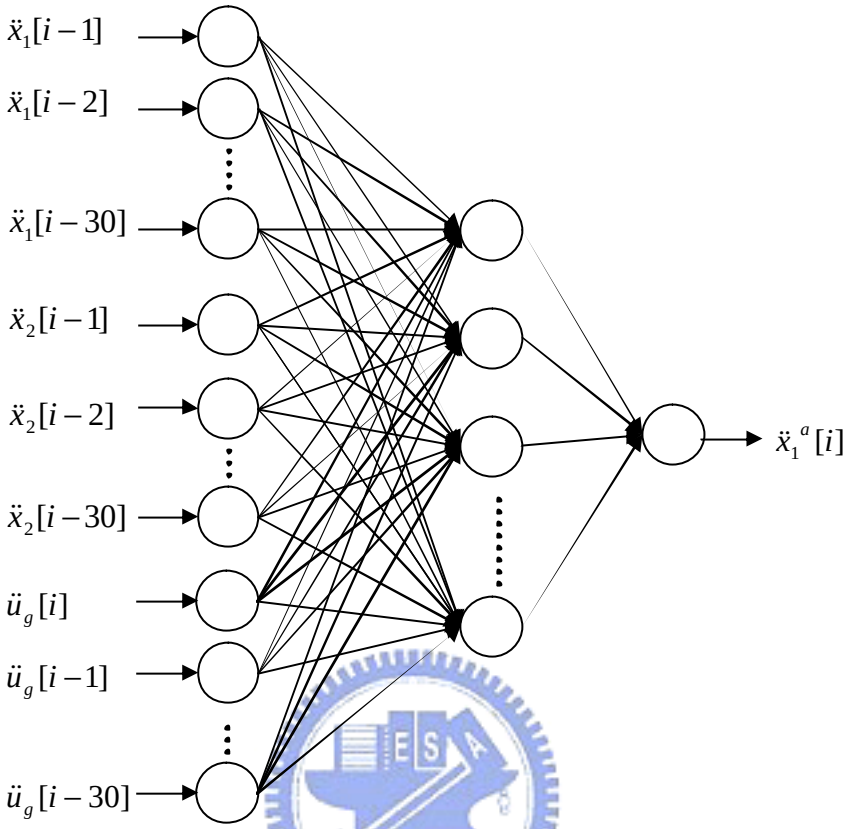

Figure 4.11 Topology of the neural network, Net_1

After all decentralized monitoring networks are trained with the corresponding responses from a healthy structure the trained networks are then fed with the responses from the same structure under different damage cases listed in Table 4.3 to monitor the conditions of the structure. Moreover, basing on the properties that exhibited by the network performance, the conditions of prediction error from each network due to the occurrence of damage are summarized in Table 4.4. Herein, the predicted output error is defined as the MAE (equation (4.38)) between the forecasting and the measured responses.

Table 4.4 The conditions of predicted output error for each network due to the occurrence of damage

Damage condition	**Predicted output error increases in network**
Stiffness reduction in k_1	Net_1
Stiffness reduction in k_2	Net_1 &Net_2
Stiffness reduction in k_3	Net_2 &Net_3
Stiffness reduction in k_4	Net_3 &Net_4
Stiffness reduction in k_5	Net_4 &Net_5
Stiffness reduction in k_6	Net_5 &Net_6

Figures 4.12 to 4.16 show the predicted results of the decentralized monitoring networks for each damage case. When look through the results shown in these figures, the identification of damage is consistent with the descriptions listed in Table 4.4 except for the Case 1. Furthermore, the network with maximum *MAE* just indicates the damage location. For example, the damage locations for Case 2 and Case 3 are in the 2nd and 3rd story, respectively, and the network with the maximum *MAE* for these two cases are just Net_2 and Net_3, respectively.

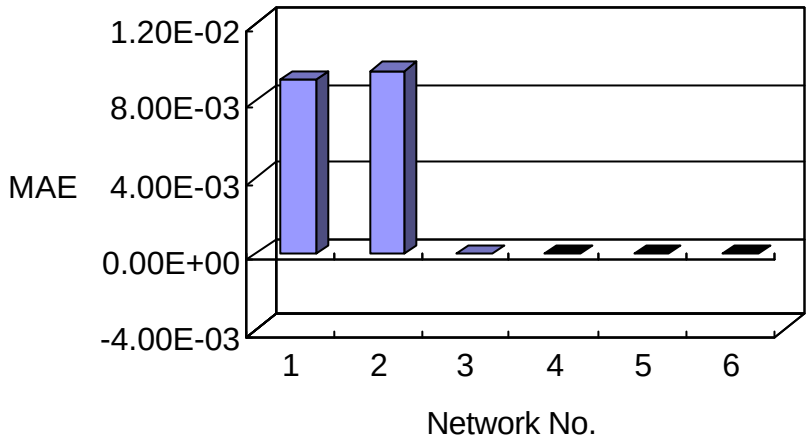

Figure 4.12 Predicted *MAE* for Case 1

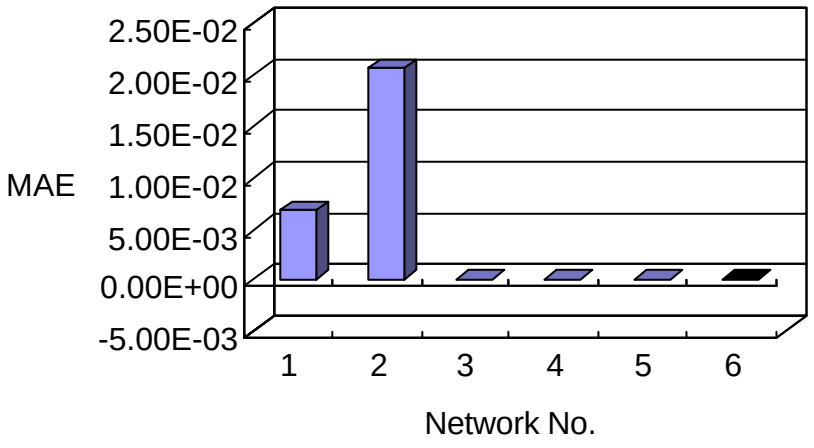

Figure 4.13 Predicted *MAE* for Case 2

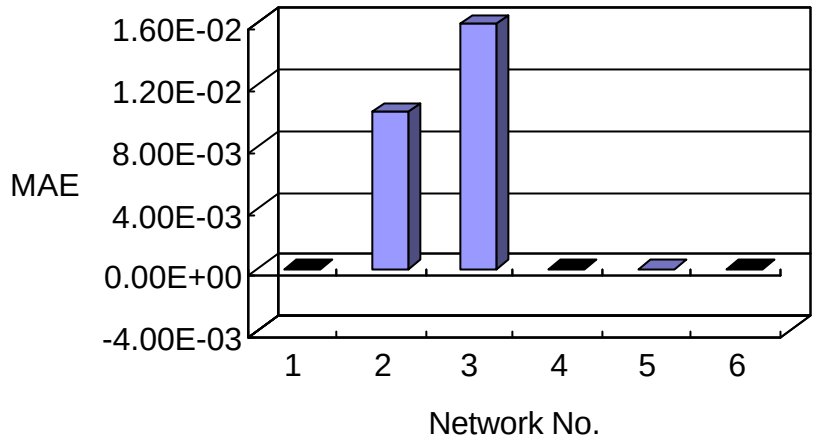

Figure 4.14 Predicted *MAE* for Case 3

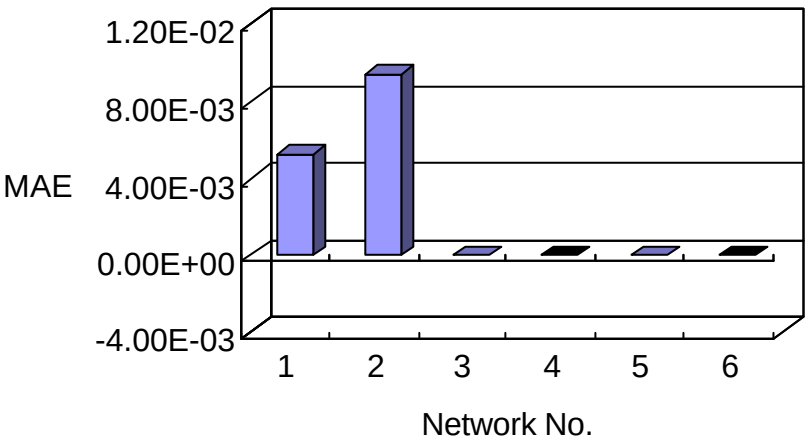

Figure 4.15 Predicted *MAE* for Case 4

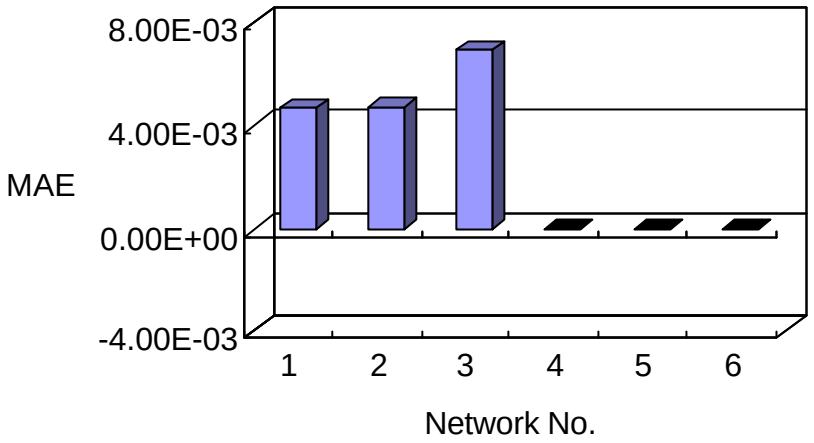

Figure 4.16 Predicted *MAE* for Case 5